Rotation and Fast Marching Based Shape Recovery of Multiple Color Object

Yuji IWAHORI†, Yi DING††, Tsuyoshi NAKAMURA†††, Robert J. WOODHAM††††, and Lifeng HE†††††

† Chubu University Matsumoto-cho 1200, Kasugai 487-8501, Japan
†† Wuxi City College of Vocational Technology Qianou Road No.12, Wuxi 214-000, China
††† Nagoya Institute of Technology Gokiso-cho, Showa-ku, Nagoya 466-8555, Japan
†††† University of British Columbia Vancouver, B.C. Canada, V6T 1Z4
††††† Aichi Prefectural University Aichi 480-1198, Japan
E-mail: †iwahori@cs.chubu.ac.jp, ††dingyi.dl@gmail.com, †††tnaka@nitech.ac.jp, ††††woodham@cs.ubc.ca, †††††helifeng@ist.aichi-pu.ac.jp

Abstract This paper proposes a new approach to recover the 3-D shape of multiple color object via rotation. Many empirical photometric approaches use a calibration object. In general, multiple light sources allow one to recover both the color reflectance and the shape of a target object. Here, a new Fast Marching Method (FMM) algorithm is proposed to recover 3-D shape for the case of a single parallel light source aligned with the viewing direction. Color reflectance factors based on a dichromatic reflectance model are estimated using clustering. Subsequently, a Lambertian shaded image is generated using a conversion table. Experiments with both synthetic and real data are demonstrated.

Key words Fast Marching Method, Self-Calibration, Color Reflectance Factor

1. Introduction

3-D shape recovery is an important research topic in computer vision, with many practical applications. Woodham [1] introduced photometric stereo as a method to recover surface orientation from multiple shaded images. Later, an entirely empirical approach to photometric stereo [2] was demonstrated. Subsequently, Hertzmann and Seitz [3] relaxed the requirement that the calibration object have exactly the same reflectance properties as the target object. The goal of that work was to recover both shape and surface reflectance, for application to computer graphics.

Iwahori *et al.* [4] developed a neural network (NN) implementation of photometric stereo. Iwahori *et al.* [5] introduced a method to obtain a virtual calibration sphere by controlled, one degree of freedom (DOF) rotation of the target object itself, calling this self-calibration.

Kimmel and Sethian [6] formulate the image irradiance equation as an eikonal equation and solve it with Sethian's Fast Marching Method (FMM) [7]. Lambertian reflectance was assumed. Iwahori *et al.* [8] extended the FMM approach to handle monotonic, non-Lambertian reflectance. Shape is recovered with the FMM by generating a lookup table, via self-calibration, to convert to an equivalent Lambertian reflectance, while [9] is a further extension of FMM under a point light source illumination and perspective projection. However, the approaches taken in [8] [9] still assume a single reflectance function for all points on the target object.

The empirical approaches in [2]〜[4] all use explicit calibration objects of known shape, a sphere in [2], [4], spheres and cylinders in [3]. Multiple light source directions are required. In this paper, the FMM is further extended using a conversion table. Self-calibration and k-means clustering make it possible to recover spatially varying color reflectance factors, based on a dichromatic reflectance model. The FMM thus is extended to handle multi-colored objects.

2. Previous Work

2. 1 FMM

Assume a single, parallel light source. Let $\boldsymbol{s}$ be a unit vector in the light source direction. Let $\boldsymbol{n}$ be a unit surface normal vector. Let $\boldsymbol{v}$ be a unit vector in the viewing direction. Assume that the light source direction is aligned with the viewing direction and that both are aligned with the z axis so that $\boldsymbol{s} = \boldsymbol{v} = (0, 0, 1)$. Image irradiance, E, for Lambertian reflectance becomes

$$E = \rho(\boldsymbol{s} \cdot \boldsymbol{n}) = \rho \frac{1}{\sqrt{p^2 + q^2 + 1}} \qquad (1)$$

where ρ is a reflectance factor, $z(x, y)$ is the depth distribution, and (p, q) is the surface gradient given by $p = \frac{\partial z}{\partial x}$ and $q = \frac{\partial z}{\partial y}$. Eq.(1) can be rewritten as

$$\sqrt{p^2 + q^2} = \sqrt{\frac{\rho^2}{E^2} - 1} \qquad (2)$$

Eq.(2) is of the form $|\nabla z(x, y)| = f(x, y)$ and is an eikonal equation. The FMM is one approach to solve an eikonal equation fast. The FMM algorithm is described as follows (see Fig.1):

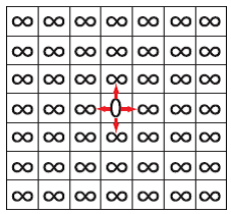

(a) Initialization

$known\{0\}, far\{\infty\}$,
$trial\{\ \}$

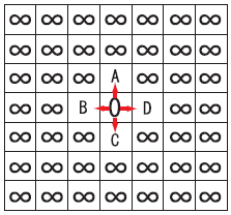

(b) Determining 4 nearest neighbor points
$known\{0\}, far\{\infty\}$,
$trial\{A, B, C, D\}$

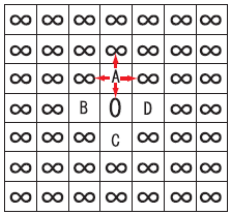

(c) Selecting minimum points among ABCD
$known\{0, A\}, far\{\infty\}$,
$trial\{B, C, D\}$

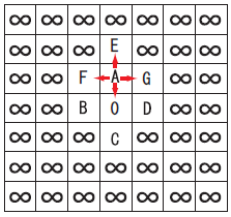

(d) Determining temporal value of 4 nearest points
$known\{0, A\}, far\{\infty\}$,
$trial\{B, C, D, E, F, G\}$

Fig. 1 FMM

Step 1 (Initialization). (Fig.1(a)) All pixels are labeled as one of three lists, $known, trial, far$, according to the following processes:

(1) First pixel is added to $known$ list. Z is assigned to 0.

(2) Four nearest neighboring points not $known$ are labeled as $trial$ and Z is assigned to f_{ij}.

(3) Other pixels are added to far list. Z is assigned as ∞.

Step 2. (Fig.1(b)) Select a pixel (i_{min}, j_{min}) with the minimum value of Z among $trial$ list and remove the pixel from $trial$ list and add it to $known$ list.

Step 3. (Fig.1(c)) Pixels which belong to far list among four neighboring points around (i_{min}, j_{min}) are added to $trial$ list.

Step 4. (Fig.1(d)) Z of the nearest neighboring points of pixel (i_{min}, j_{min}), which belongs to $trial$ list, is calculated and registered.

Step 5. If the $trial$ list is empty, exit the procedure. Otherwise, return to Step 2.

2. 2 Self-Calibration

The FMM has been applied when the reflectance function does not vary from point to point on the target object. The effects of a spatially varying color reflectance factor and specular reflection still need to be taken into account. In [5], target object images are acquired over a full, 360 degree, one DOF rotation with a single light source. Reflectance properties are measured from the target object itself.

At points on the occluding boundary of the target object, the surface normal is perpendicular to both the tangent to the occluding boundary and the viewing direction. Accordingly, the surface normal, $\boldsymbol{n}$, at points on an occluding boundary is uniquely determined by the local geometry. These known points are tracked during rotation and the corresponding surface normal, $\boldsymbol{n}$, at any rotation angle is thus also determined.

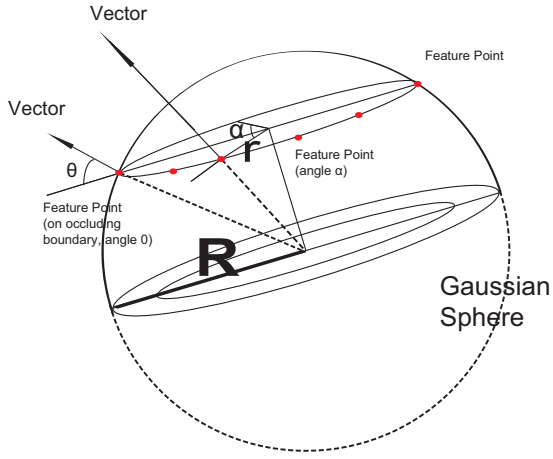

Fig. 2 Gaussian Sphere and Feature Point

Gaussian sphere is defined as a virtual sphere with its radius $R = 1$. θ represents the angle between the normal vector of the feature point and the horizontal axis (as shown in **Fig.2**).

From the relation of neighboring points for the triangles in **Fig.3** and **Fig.4**, the surface normal, $\boldsymbol{n}$, of the current feature point is determined using the $\cos\theta$. $\cos\theta$ takes plus or minus value. If the vector $\boldsymbol{n}$ is over the horizontal axis, $\cos\theta$ takes plus value. If the vector $\boldsymbol{n}$ is under the horizontal axis, $\cos\theta$ takes minus value (as shown in **Eq.3** and **Eq.4**).

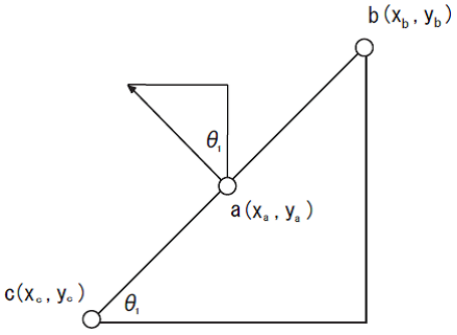

Fig. 3 Feature Point (a)

$$\cos\theta_1 = \frac{x_c - x_b}{\sqrt{(x_c - x_b)^2 + (y_c - y_b)^2}} \tag{3}$$

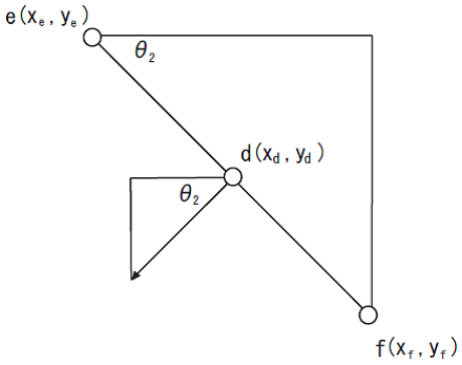

Fig. 4 Feature Point (b)

$$\cos\theta_2 = \frac{x_e - x_f}{\sqrt{(x_e - x_f)^2 + (y_e - y_f)^2}} \tag{4}$$

Except the points on the occluding boundary, the $\boldsymbol{n}$ are given by

$$n_x = \cos\theta\cos\alpha \tag{5}$$

$$n_y = \sin\theta \tag{6}$$

$$n_z = \cos\theta\sin\alpha \tag{7}$$

where α is the current rotation angle.

In the end, a set of surface normals and corresponding image irradiances is obtained. (For details, see [5]).

2.3 Dichromatic Reflectance Model

The dichromatic reflectance model considers image irradiance, E, to consist of two components, one for diffuse (Lambertian) reflection, E_d, and one for specular reflection, E_m. The color of the diffuse component represents the color of object itself, while the color of the specular component represents the color of light source. The relative contribution of E_d and E_m depends on $\boldsymbol{n}$, $\boldsymbol{s}$ and $\boldsymbol{v}$ at each surface point.

$$E = E_d(\boldsymbol{n}, \boldsymbol{s})\rho + E_m(\boldsymbol{n}, \boldsymbol{s}, \boldsymbol{v}) \tag{8}$$

where ρ again is the object's (diffuse) reflectance factor.

3. Color Clustering and Reflectance Factors

To apply the FMM to a multiple colored object, it is necessary first to obtain color reflectance factors, ρ_i, $i = \mathrm{R}, \mathrm{G}, \mathrm{B}$. According to Eq.(8), the color reflectance factor at any target point can be calculated as

$$\rho_i = (E_i - E_{im})/E_{id}, \quad i = \mathrm{R}, \mathrm{G}, \mathrm{B}.$$

The diffuse components, E_{id}, can be calculated from the cosine of the incident angle (i.e., the angle between $\boldsymbol{n}$ and $\boldsymbol{s}$). Recall, the light source direction and viewing direction are assumed aligned so that, at all target points, $\boldsymbol{s} = \boldsymbol{v} = (0, 0, 1)$. Image irradiances, E_i, and the corresponding surface normal vector, $\boldsymbol{n}$, are obtained for selected target points during self-calibration.

We are interested in estimating color reflectance factors, ρ_i, at all target points. To address this problem, points are classified based on a clustering of color feature vectors into a fixed, finite number of color equivalence classes. Normalized color coordinates ($R_n = R/Y, G_n = G/Y, B_n = B/Y$) are used to make the color clustering simpler, where Y is the monochrome image irradiance as follows: $Y = 0.299\times R + 0.587\times G + 0.114\times B$. Fig.6 shows a plot of (R, G, B) data and the associated (R_n, G_n, B_n) data.

K-means algorithm is used to cluster colors, where k is given *a priori*. Here, k means the number of colors. k becomes the number of colors of feature points, which is equal to the number of colors of the target object. After the number of colors of feature points are determined, the number of colors k is given.

First, intensities of feature points are observed in HSV color space. $\boldsymbol{H}$ (Hue) is one of the main properties of color. Observing kinds of $\boldsymbol{H}$ gives the number of colors k. Here the intensities of feature points are converted from RGB color space to HSV color space using conversion equation. For easy observation, $\boldsymbol{H}$ of feature points are sorted, shown in Fig.5. When H in Fig.5 suddenly changes, H of one color is recognized. In this case, k is determined as 5.

After k-means clustering is applied, the color reflectance factors for an arbitrary point are taken to be those of the mean of the cluster to which the point belongs.

A standard k-means clustering algorithm is used. Clustering is applied to each RGB component and color

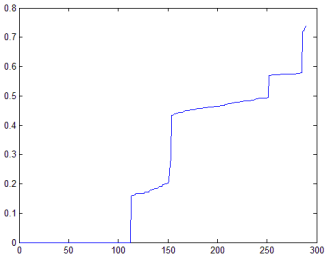

Fig. 5 Sorted Data for $\boldsymbol{H}$

reflectance factors of all points on the object are thus estimated. An example of color clustering for a real test object is shown in Fig.7.

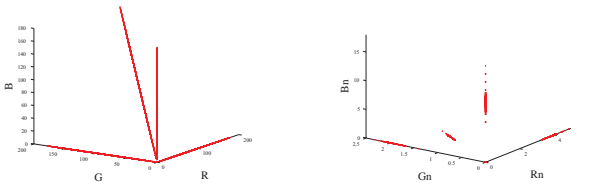

(a) (R, G, B) Space (b) (R_n, G_n, B_n) Space

Fig. 6 Sample Data Distribution

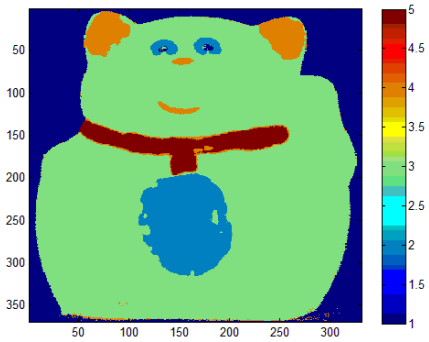

Fig. 7 Example of Color Clustering

4. Conversion Table for Color Textured Object

A conversion table is generated during self-calibration to transform actual measured irradiances of tracked feature points to those of an equivalent Lambertian reflector.

Feature points which lie on the equator line of a virtual sphere are used to construct the conversion table. This ensures that there will be one rotation angle at which the feature point is brightest (i.e., $\boldsymbol{n} = \boldsymbol{s}$).

As the target object is rotated from -90 to 90 degrees, the corresponding image irradiances, E, are recorded in the conversion table together with the associated rotation angle. Along the equator of the virtual sphere, the conversion table maps the recorded value of image irradiance, E, to the corresponding ideal value for Lambertian reflectance. The generated conversion table is used to interpolate Lambertian irradiance values from the observed E. Here, E should be monotonically increasing from -90 to 0 degrees rotation and monotonically decreasing from 0 to 90 degrees rotation. Only feature point data that satisfy this condition are used to construct the conversion table.

The specular reflection component and the color reflectance factor are removed from E, based on the dichromatic reflectance model, as follows. The specular component includes points which have image irradiance, E, over a threshold and with a sudden large change of gradient. These points are removed from consideration. The remaining points are used to estimate the diffuse reflection component. Cubic spline interpolation is applied to these data. Then the diffuse component, $E_d\rho$, is separated from E. The overall specular component is estimated as $E_m = E - E_d\rho$.

For multi-colored objects, the conversion table is applied separately to each color region. To construct the conversion table itself, the effect of the reflectance factor is first removed by computing an adjusted image irradiance $E^{'} = \frac{E - E_m}{\rho_1}$ where ρ_1 represents the reflectance factor of the brightest feature point. For the given color region, $E^{'}$ is multiplied by the reflectance factor, ρ_i, of the associated color region to produce $E^{''} = E^{'}\rho_i + E_m$. $E^{''}$ then is used for the conversion table.

As shown in Fig.8, input (horizontal axis) of the conversion table is the target object image irradiance. Output (vertical axis) is the corresponding Lambertian image irradiance.

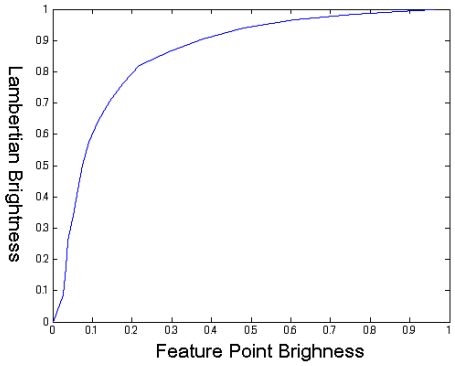

Fig. 8 Lambertian Conversion Table for One Color Region

The overall algorithm is summarized as follows:

Step 1. Acquire 37 images stepped 5 degrees in rotation over the range -90 to 90 degrees.

Step 2. Apply K-means algorithm for color clustering.

Step 3. Separate specular components using cubic spline interpolation.

Step 4. Calculate surface normal of feature points.

Step 5. Calculate color reflectance factors of feature points using dichromatic reflectance model.

Step 6. Recover color reflectance factors for all object points according to the values in the associated cluster region.

Step 7. Generate conversion table (from object reflectance to Lambertian) from feature points.

Step 8. Generate (idealized) Lambertian image of target object using conversion table.

Step 9. Use the Fast Marching Method algorithm to recover 3-D shape from the Lambertian image.

5. Experiments

5.1 Computer Simulation

A Phong reflectance model is used. Image irradiance, E, is

$$E_j = 255 \times (\rho_j \cos i + t \cos^n s), \quad j = \mathrm{R}, \mathrm{G}, \mathrm{B}.$$

where ρ_j is the color reflectance factor for (R, G, B), s is the off-specular angle, i is the incident angle, and t are the overall weight of the specular component compared to the diffuse component, $(0 \leqq t \leqq 1)$, and $n > 0$ is a parameter that determines the concentration (i.e., effective width) of the specular component.

In the simulation, $t = 0.4$ and $n = 15$. One of the multi-colored synthetic input images is shown in Fig.9-(a). Simulation incorporates the expected effect of noise by adding 3% Gaussian noise to each input image. The vase-like shape is defined mathematically by

$$r = 0.9 \sin x + 1.3$$
$$z = \sqrt{r^2 - y^2}$$

where $-\pi < x < 9\pi/2$, and $-0.9 \sin x - 1.3 < y < 0.9 \sin x + 1.3$.

For self-calibration, 37 images were synthesized and the object rotated in 5 degree increments over the range -90 to 90 degrees. These images were used to generate the conversion table and to estimate color reflectance factors. Fig.9-(b) shows the generated Lambertian image. Fig.9-(c) shows the color reflectances.

The actual mathematically defined surface is shown in Fig.9-(d). The maximum height of the true shape is

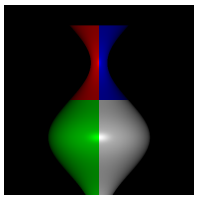

(a) Input Image

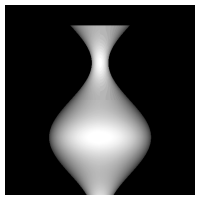

(b) Lambertian Image

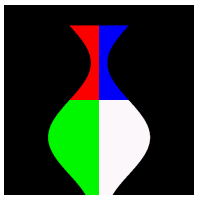

(c) Color Reflectance

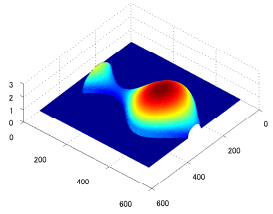

(d) Actual Surface

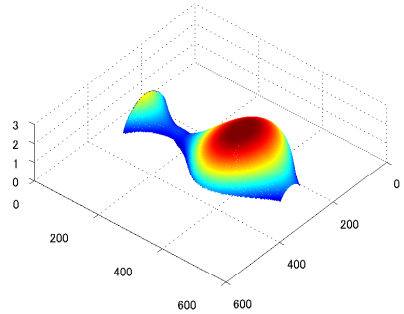

(e) 3-D Shape Using FMM

Fig. 9 Example of Phong Model

2.2. The shape recovered using FMM is shown in Fig.9-(e). The mean error is 0.0163 and the maximum error is 0.1854. Compared to the true shape, the recovered result is is both qualitatively and quantitatively accurate. The mean error of that method is 0.1237 and the maximum error is 0.5165.

5.2 Experiment with a Real Object

A real test object is shown in Fig.10-(a). Color images were acquired and converted to monochrome as follows:

$$E = 0.299 \times E_R + 0.587 \times E_G + 0.114 \times E_B$$

The monochrome image is shown in Fig.10-(b). The generated Lambertian image is shown in Fig.10-(c). Estimated color reflectance factors are shown in Fig.10-(d). The recovered 3-D shape is shown in Fig.10-(e).

Separation of specular components used 37 images (from -90 to 90 degrees), and generation of the conversion table used 19 images (from -90 to 0 degrees), 5 degrees of rotation apart. Thus, the number of images now required is reduced.

To obtain the result shown in Fig.10-(e), initial heights are given to two points on the target object,

(a) Real Object

(b) Monochrome Image

(c) Lambertian Image

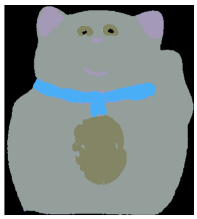

(d) Color Reflectance

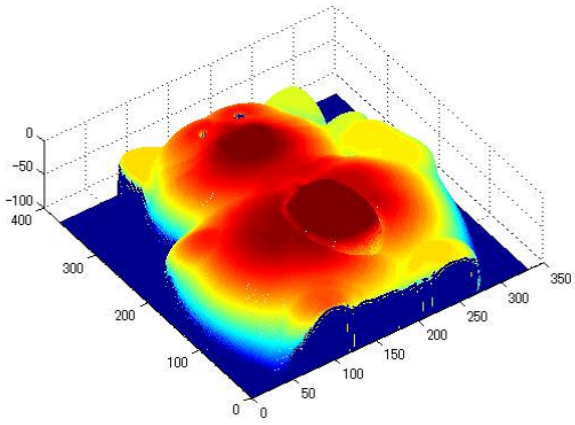

(e) 3-D Shape Using FMM

Fig. 10 Results for Real Object

one at the top of the mouth and the other at the top of the body. These initial heights were estimated during calibration.

Experiments were done with an Intel Core2Duo 2.2GHz CPU with 2GB memory. Following calibration, shape recovery with the FMM algorithm took 1.3 [sec],

The method uses k-means clustering to segment colors. This is most effective when the colors on the target object are distinct and the number of colors is known. Clustering likely will fail if there is gradation (i.e., blending) of color or if the number of colors is large and unknown. The FMM algorithm assumes smoothness and thus cannot handle surface discontinuities. Concave regions also cause difficulties owing to self-occlusion during rotation.

6. Conclusion

This paper demonstrates a new approach to recover the 3-D shape of multi-colored objects. Self-calibration, color clustering, a conversion table and the Fast Marching Method (FMM) combine to recover both color reflectance factors and 3-D shape. Self-calibration determines image irradiances and the corresponding surface normal at selected target points. Rotation of the object is used and all images are acquired with a single light source direction aligned with the viewer. K-means clustering segments color regions and allows recovery of color reflectances from the dichromatic reflectance model. A conversion table estimates the ideal Lambertian image to which a FMM algorithm is applied. Acceptable results were obtained on both synthetic and real data. Concave regions are problematic since self occlusion arises during calibration, limiting the ability to track known feature points. Dealing with concavity is a subject for future work.

Acknowledgements

The authors thank our undergraduate student Satoki Yanagisawa for his experimental help. Iwahori's research is supported by JSPS Grant-in-Aid for Scientific Research (C) (23500228) and Chubu Univ. Grant. Woodham's research is supported by NSERC.

References

[1] R. J. Woodham, "Photometric Method for Determining Surface Orientation from Multiple Images," Opt. Engineering, Vol.19, pp.139–144, 1980.

[2] R. J. Woodham, "Gradient and Curvature from the Photometric Stereo Method, Including Local Confidence Estimation," J. Opt. Soc. Am., A, Vok.11, pp.3050–3068, 1994.

[3] A. Hertzmann and S. M. Seitz, "Example-Based Photometric Stereo: Shape Reconstruction with General, Varying BRDFs," IEEE Trans. on PAMI, Vol.27, No.8, pp.1254–1264, 2005.

[4] Y. Iwahori, R. J. Woodham, M. Ozaki, H. Tanaka, and N. Ishii, "Neural Network Based Photometric Stereo with a Nearby Rotational Moving Light Source," IEICE Trans. on Information and Systems, Vol.E80-D, No.9, pp. 948–957, 1997.

[5] Y. Iwahori, Y. Watanabe, R. J. Woodham and A. Iwata, "Self-Calibration and Neural Network Implementation of Photometric Stereo," Proc. 16th ICPR, Vol.4, pp.359–362, 2002.

[6] R. Kimmel and J. A. Sethian, "Optimal Algorithm for Shape from Shading and Path Planning," J. Math. Imaging and Vision, Vol.14, pp.237–244, 2001.

[7] J. A. Sethian, "A Fast Marching Level Set Method for Monotonically Advancing Fronts," Proc. Nat. Acad. Sci., Vol.93 No.4 pp.1591–1595, 1996.

[8] Y. Iwahori, T. Nakagawa, R. J. Woodham, S. Fukui, H. Kawanaka: "Shape from Self-Calibration and Fast Marching Method," Proc. ICPR2008, pp.1–4, 2008.

[9] Y. Iwahori, K. Iwai, R. J. Woodham, H. Kawanaka, S. Fukui, K. Kasugai: "Extending Fast Marching Method under Point Light Source Illumination and Perspective Projection," Proc. ICPR2010, pp.1650-1653, 2010.